Published in final edited form as:
Nature. 2009 December 17; 462(7275): 880–885. doi:10.1038/nature08616.

Transport mechanism of a bacterial homologue of glutamate transporters

Nicolas Reyes, **Christopher Ginter**, and **Olga Boudker**
Department of Physiology and Biophysics, Weill Cornell Medical College 1300 York Ave, Box 75, New York, New York 10065, USA

Abstract

Glutamate transporters are integral membrane proteins that catalyze a thermodynamically uphill uptake of the neurotransmitter glutamate from the synaptic cleft into the cytoplasm of glial and neuronal cells by harnessing the energy of pre-existing electrochemical gradients of ions. The linchpin of the reaction is the conformational transition of the transporters between outward and inward facing states, in which the substrate binding sites are accessible from the extracellular space and the cytoplasm respectively. Here we describe a crystal structure of a double cysteine mutant of a bacterial homologue of glutamate transporters, Glt_{Ph}, which is trapped in the inward facing state by cysteine cross-linking. Together with the previously determined crystal structure of Glt_{Ph} in the outward facing state, the structure of the cross-linked mutant allows us to propose a molecular mechanism, by which Glt_{Ph} and, by analogy, mammalian glutamate transporters, mediate sodium-coupled substrate uptake.

Glutamate is the predominant excitatory neurotransmitter in the brain responsible for learning, memory formation and higher cognitive function. Specialized membrane proteins, glutamate transporters, also termed excitatory amino acid transporters (EAATs), mediate the transmitter uptake from the extracellular space into the cytoplasm of astrocytes and neurons against steep concentration gradients to allow for rounds of neurotransmission and to prevent glutamate-mediated excitotoxicity[1]. EAATs are members of a ubiquitous SoLute Carrier 1 (SLC1) family of secondary solute transporters2, which catalyze concentrative uptake of the acidic and neutral amino acids and dicarboxylic acids in a reaction coupled to symport of sodium and/or protons and, in the case of EAATs, antiport of potassium. The conceptual mechanisms of protein-mediated solute transport were developed over 40 years ago[3–5] and focus on the ability of transporters to undergo isomerization between two states: an outward facing state, in which the substrate-binding site is accessible from the external solution, and an inward facing state, in which it is reached from the cytoplasm. Although our understanding of the molecular mechanisms of transport have advanced significantly in the last decade[6,7], the structural transitions between the outward and inward facing states remain poorly characterized.

The sodium/aspartate symporter from *Pyrococcus horikoshii* (Glt_{Ph}), an archaeal homologue of the EAATs, was one of the first sodium-coupled transporters whose structure had been determined at a near atomic resolution[8,9]. The structural analysis of Glt_{Ph} revealed that

Correspondence. Correspondence and requests of materials should be addressed to O.B. (olb2003@med.cornell.edu)..
Author contributions. N.R. and O.B. designed the project. N.R. performed protein purification, cross-linking, crystallization and structure determination. C.G. performed cloning, cell culture and protein purification. N.R. and O.B. wrote the manuscript.

Supplementary Information Description. Supplementary Information, including 4 Supplementary Figures, Supplementary Table and Supplementary Movie, accompanies the paper.

Coordinate Deposition. The coordinates for the structure and the structure factors are deposited in the Protein Data Bank under accession code 3KBC.

individual protomers assemble into a homotrimer, forming a deep solvent-filled bowl open to the extracellular solution and reaching approximately half way across the lipid bilayer (Fig. 1a). The first six transmembrane segments (TMs) of each Glt_{Ph} protomer mediate all inter-subunit contacts and form a distorted cylinder within which the highly conserved carboxyl terminus of the protein is folded into a compact core. The core consists of an intracellular re-entrant helical hairpin (HP) 1, TM7 with an unwound segment, an extracellular hairpin, HP2, and an amphipathic TM8. Despite the trimeric assembly, shared by all characterized glutamate transporter homologues[10–12], protomers function independently[13–17]. Consistently, in Glt_{Ph} crystal structure an L-asp molecule and two sodium ions are bound within the core of each individual protomer. Positioned between the tips of HP1 and HP2 at the bottom of the extracellular bowl, the substrate is occluded from the aqueous milieu only by HP2. Strikingly, in a crystal structure of Glt_{Ph} in complex with a competitive blocker, L-threo-β-benzyloxyaspartate (L-TBOA)[9,18], HP2 assumes an open conformation, revealing its dynamic nature and suggesting that it may serve as an extracellular gate. Bound L-asp and L-TBOA are separated from the cytoplasm by over 15 Å of a compact protein core, suggesting that these structures correspond to the outward facing state of the transporter. However, the structure of the inward facing state and the manner in which the substrate and sodium ions are released into the intracellular solution, remain unknown.

Cross-linking cysteines in TM2 and HP2

In a study predating the crystal structure determination of Glt_{Ph}, Vandenberg and colleagues reported that two cysteines placed in TM2 and HP2 of EAAT1 formed a spontaneous disulfide bond suggesting close proximity of these residues[19]. Strikingly, in the crystal structures of L-asp and L-TBOA-bound Glt_{Ph} the corresponding residues K55 in TM2 and A364 in HP2 are over 25 Å apart and cysteines at these positions are unlikely to become cross-linked. Moreover, the inter-subunit residue-to-residue distances are also 25–30 Å (Fig. 1a). Intrigued by these results, we reasoned that TM2 and HP2 become juxtaposed in an as yet structurally uncharacterized functional state of the transporter and set out to reproduce the double cysteine mutation in Glt_{Ph} for crystallographic studies. The K55C/A364C mutant was generated within a cysteine-less Glt_{Ph}, expressed in *E. coli* and purified in detergent solution. Oxidative cross-linking of Glt_{Ph}-K55C/A364C in the presence of copper 1,10-phenantroline (CuPhen) yielded distinct protein species with a higher electrophoretic mobility on SDS PAGE (Fig. 1b), which we identified as intramolecularly cross-linked Glt_{Ph} protomers (Supplementary Fig. 1a–c). Interestingly, CuPhen-catalyzed disulfide bond formation is greatly facilitated when the transporter is purified in the absence of sodium ions (Na^+) and L-asp, suggesting that the state in which residues 55 and 364 are proximal, is more populated under these conditions (Fig. 1b and Supplementary Fig. 2a). Qualitatively similar results were also obtained using unpurified K55C/A364C mutant within *E. coli* crude membranes, demonstrating that Glt_{Ph}, like EAAT1, adopts the new conformation in the context of a lipid bilayer. Moreover, cysteines at structurally adjacent positions did not form a disulfide bond, suggesting that the distance shortening between positions 55 and 364 occurs in a highly specific manner (Ref. 19 and Supplementary Fig. 2b). Strikingly, incubation of Glt_{Ph}-K55C/A364C with divalent mercury (Hg^{2+}), which serves as a bi-functional thiol-specific cross-linker, yields an essentially complete cross-linking both in the presence and in the absence of Na^+ and L-asp in detergent and in crude membranes (Fig 1c). Furthermore, cross-linking is completed within seconds, suggesting that both substrate-free and bound Glt_{Ph} rapidly sample the crosslinking-competent state.

Crystal structure determination

Hg^{2+}-cross-linked K55C/A364C mutant (Glt_{Ph}-$55C/364C_{Hg}$) in the presence of Na^+ and L-asp yielded crystals diffracting to 3.5–3.9 Å (See Supplementary Table 1). A previous extensive study, conducted by Slotboom and colleagues, has suggested that the functionally relevant

conformational transitions of a related bacterial glutamate transporter do not involve regions engaged in protein trimerization, because cross-linking of multiple interfacial residues had no effect on substrate transport[17]. Hence, we used a trimeric Glt_{Ph} model comprised of TM-s 2, 4 and 5, which are responsible for all inter-subunit contacts (Fig. 1a), to search for a molecular replacement solution. The initial phases yielded distinct peaks within the anomalous difference Fourier map corresponding to Hg atoms at positions adjacent to cysteines 55 in TM2. Rounds of manual building and refinement resulted in a protein model lacking 5 and 8 residues on the amino and carboxyl termini, respectively, and including 98 % of the side chains. To verify the model, we crystallized the selenomethionine-substituted Glt_{Ph}-55C/364C_{Hg}. The Se peaks within the anomalous difference Fourier maps are in perfect agreement with the location of 17 methionines in the protein model (Supplementary Fig. 3a). The distance between the Cα atoms of modelled cysteines 55 and 364 is 7.4 Å, and the Hg peak within the anomalous difference Fourier map is positioned between these residues with the sulphur to mercury distances estimated at 2 – 2.3 Å (Supplementary Fig. 3b), similar to those observed in small molecular weight compounds[20] and peptides[21, 22].

Structure of the inward facing state

The most striking structural feature of Glt_{Ph}-K55C/364C_{Hg} compared to the WT Glt_{Ph}, is a ca 18 Å movement of the substrate binding sites from near the extracellular solution at the bottom of the extracellular bowl, to near the cytoplasm (Figs. 2a, b). Structural superposition using trimerization TM-s 2, 4 and 5, along with the peripheral TM1 reveals that these segments remain largely unchanged, with the root mean square deviation (RMSD) for the atomic positions of 1.2 Å. The remainder of the protein, including TMs 3 and 6, HP1, TM7, HP2 and TM8, does not align and has undergone a substantial movement (Fig. 2a). Remarkably, when these regions alone are superposed, their structures are essentially identical, yielding RMSD of 0.6 Å. These results suggest that Glt_{Ph} can be partitioned into two structural domains, which we termed the trimerization and transport domains (Fig. 2c). The rigid body movements of the transport domains relative to the trimerization domain dominate the structural changes between the substrate-bound WT Glt_{Ph} and Glt_{Ph}-55C/364C_{Hg} (Fig. 2a,b and Supplementary Movie). The structural environment of the ion- and substrate-binding sites, which are positioned entirely within the transport domains, is preserved. The Fo-Fc difference Fourier map reveals excess electron density at these sites (Supplementary Fig. 4), suggesting that the transporter remains bound to L-asp and to two Na^+ ions. Consistently, substrate-free Glt_{Ph}-55C/364C_{Hg} in solution binds L-asp with high affinity and in a sodium-dependent manner (Fig 2d). In the structure of Glt_{Ph}-55C/364C_{Hg} the substrate binding sites lie near the bottom of deep crevices formed within each protomer between HP1 and the cytoplasmic portion of TM7 of the transport domain and TMs 2 and 5 of the trimerization domain (Fig. 2b). Bound L-asp and Na1 are completely occluded from the solution by the tips of HP1 and HP2, while Na2 is partially exposed to the solvent (Fig. 2a, b). Because substrate and ion binding sites are near the intracellular solution, we propose that the conformation of Glt_{Ph}-55C/364C_{Hg} corresponds to an inward facing state of the transporter.

Because the trimerization domain undergoes little conformational transitions, it is unlikely to change its position relative to the membrane plane. Hence, we estimate that a ~25 Å thick apolar region of the lipid bilayer, which in the WT Glt_{Ph} aligns approximately with the hydrophobic portion of TM1, is similarly positioned in Glt_{Ph}-55C/364C_{Hg}. Such bilayer placing suggests that several polar residues at the extracellular ends of the lipid-facing TMs 3 and 6 move into the hydrophobic region of the membrane. It is possible that the lack of the lipid bilayer in the crystals removes important constrains, resulting in a non-native positioning of the transport domain. However, cross-linking of residues 55C and 364C in Glt_{Ph} and corresponding residues in EAAT1 occurs efficiently in lipid membranes, suggesting that a sufficient range of motions of the transport domain is allowed. Movement of the transport

domain toward the cytoplasm also significantly increases its exposure to the intracellular solvent. Strikingly, although the total exposed cytoplasmic surface area increases from ~1,300 in the WT to ~4,200 Å^2 in the Glt_{Ph}-55C/364C_{Hg}, the fraction of the apolar area changes only modestly from 57 to 63 %. Both values are well within the range reported for the solvent exposed area of soluble proteins[23].

Domain interaction interfaces

Both WT Glt_{Ph} and Glt_{Ph}-55C/364C_{Hg} bury approximately equal surface areas of ~2,500 Å^2 on the interface between the trimerization and transport domains. Furthermore, in both structures essentially the same residues of the trimerization domain are involved, forming a smooth relatively featureless interaction surface, which is over 80 % hydrophobic (Fig. 3a, b). Although TM1 and TM4 contribute to the contact area, TM2 and TM5, lying parallel to each other and crossing the membrane at an oblique angle, provide the bulk of the interactions, contributing 77 and 67 % to the interaction surface in the WT and Glt_{Ph}-K55C/A364C_{Hg}, respectively. In contrast, the transport domains in the two structures present interaction interfaces with little overlap, but similar in area (1250 Å^2) and hydrophobicity (70%). They are dominated by HP1 and the cytoplasmic portion of TM7 in the WT Glt_{Ph} (Fig. 3a), and by HP2 and the extracellular portion of TM8 in Glt_{Ph}-55C/364C_{Hg} (Fig 3b), which provide 92 and 88 % of the total buried area, respectively. The analysis of the evolutionary conservation reveals that the interacting residues within the trimerization domain as well as within the two alternative interfaces of the transport domain are all highly conserved (Fig. 3c, d). The high conservation of HP2 surface residues and the reported transport inhibition of the mammalian EAATs upon chemical modification of cysteines in HP2[24–28] are consistent with this region being involved in specific protein contacts as observed in Glt_{Ph}-55C/364C_{Hg}. The disengagement of HP1 and the amino-terminal part of TM7 and their transition to the cytoplasmic surface of the transporter is also consistent with the previously reported intracellular solvent accessibility of these regions in related prokaryotic and mammalian transporters[29–32].

It has been noted previously that the carboxyl terminal core of Glt_{Ph} contains structurally symmetrical elements[8]. Specifically, HP1 and the amino terminal half of TM7 can be superimposed on HP2 and the amino terminal portion of TM8 with RMSD of 2.5 Å. It is precisely these triplets of helices that constitute the two alternative interaction interfaces of the transport domain (Fig. 3a, b). Strikingly, also the amino terminal portion of the transporter, comprised of the first 6 TMs, exhibits a pseudo two-fold structural symmetry despite the lack of detectable sequence conservation. TMs 4 through 6 can be superimposed upon TMs 1 through 3 with RMSDs of ~6 and 4.3 Å for the WT and mutant, respectively (Fig. 4a, b). Hence, unlike other characterized secondary transporters[33–35], glutamate transporters contain not one, but two inverted structural repeats (Fig. 4d). Because of the amino-terminal symmetry, the interaction interface of the trimerization domain can be partitioned into structurally related extracellular and cytoplasmic portions (Fig. 4c), which contribute approximately equally to the total buried surface area.

Hinge movements

Within the transport domain, structurally symmetrical TM3 and TM6 serve as two arms holding the transporter core and extending from the trimerization domain, the former from the cytoplasm and the latter from the extracellular solution (Fig. 4e, f). The loops, which connect these transmembrane segments to the trimerization domain, enable the inward movement. The long flexible loop between TMs 3 and 4 is poorly structured in the L-asp-bound WT Glt_{Ph} crystals, and in Glt_{Ph}-55C/364C_{Hg} its structure is largely determined by crystal contacts. In contrast, the structurally symmetrical loops between TMs 2 and 3 and between TMs 5 and 6

are short and undergo well-defined transitions to accommodate the movements of the transport domain (Fig. 4e, f and Supplementary Movie). In Glt_{Ph}-55C/364C_{Hg}, unwinding of the TM3 α-helix by approximately one turn extends TM2–3 loop by 4 residues and allows for the descent of TM3 toward the cytoplasm. In contrast, the TM5–6 loop is shortened by 2 residues as a result of simultaneous unwinding of TM5 by a half of a turn and extension of TM6 by a turn of a helix. Both loops contain conserved glycines, G69, G79 and G82 in TM2–3 loop, and G221 in TM5–6 loop, which may facilitate the folding/unfolding of the helices and serve as hinges. Indeed, the transport domain movement can be decomposed into a 16 Å descent toward the cytoplasm followed by a 37 ° rotation around an axis passing simultaneously through the transport domain centre of mass and TM2–3 and TM5–6 loops. Consistent with the importance of the structural rearrangements in the loop regions, chemical modifications of cysteines in TM5–6 loop of EAAT3 inhibited uptake[36].

Transport mechanism

In the structure of the WT Glt_{Ph}, L-asp is bound ~5 Å beneath the surface of the extracellular bowl occluded from the solution by HP2. In contrast, in the structure of Glt_{Ph}-55C/364C_{Hg}, L-asp is bound ~5 Å beneath the intracellular surface occluded from the solution by HP1. Hence, we propose that L-asp-bound Glt_{Ph} structure corresponds to the state right after binding of the substrate from the extracellular side, *outward-facing occluded*, and Glt_{Ph}-55C/364C_{Hg} structure - to the state right before the release of the substrate into the cytoplasm, *inward-facing occluded* (Fig 5). The isomerization between these states involves a combination of a cross-membrane movement and rotation of the transport domain, comprised of the substrate-binding transporter core and peripheral TMs 3 and 6. During this movement, the lipid-facing hydrophobic TMs 3 and 6 traverse the bilayer directly, moving toward the cytoplasm by ~12 Å. In contrast, passage of the relatively polar HP1 and HP2, with their tips crossing as much as 20 Å of the lipid bilayer, is facilitated by the intra-protein track provided by the trimerization domain. The transport domains are expected to move stochastically and independently within each protomer, so that the crystal structure represents a statistically rare case, when all three transport domains are in the inward orientation. The rigid trimerization domain is anchored in the membrane and provides a counterbalance to the movements of the bulky transport domains, suggesting an explanation for the obligatory oligomeric assembly of SLC1 family of transporters.

Substrate binding/unbinding on either side of the membrane is associated with additional conformational changes, or gate openings. The crystallographic data and molecular dynamic simulations[9, 37, 38] suggest that substrate and ion dissociation on the extracellular side is associated with the opening of HP2, defining it as an extracellular gate. We hypothesize that in a functionally symmetrical manner, movements of HP1 allow for dissociation of the substrate and ions from the inward facing state, defining it as a *bona fide* intracellular gate. The alternate opening of the extracellular and intracellular gates is strictly maintained: in the outward facing state, when HP2 opens to expose the substrate and ion binding sites to the extracellular solution, HP1 is secured in the closed state, packed against TMs 2 and 5. Conversely, in the inward facing state HP2, the extracellular gate, is locked closed upon displacing HP1.

As has been suggested previously[39], coupling of the substrate transport to the energy of the ionic gradients is established via synergistic binding of substrate and sodium ions on the extracellular and intracellular sides of the membrane coupled to the closure of the corresponding gates. The steep sodium dependence of the substrate binding, observed both in WT Glt_{Ph}[9] and in Glt_{Ph}-55C/364C_{Hg} (Fig. 2d), is responsible for the differential affinity for the substrate on the extracellular side of the membrane, where sodium concentration is high, and the intracellular side, where it is low. We further propose that the isomerization between the outward and inward facing states is sodium independent and may simply be driven by the

thermal energy alone. The observation that Hg^{2+}-mediated cross-linking of K55C/A364C mutant is completed within seconds both in membranes and in detergent suggests that this transition is rapid and does not limit the rate of transport in Glt_{Ph}, which has a turnover time of ~3 minutes at ambient temperatures[40]. Finally, we hypothesize, that a similar isomerization reaction may also occur in the apo-transporter to complete the transport cycle. The structural re-arrangements within the transport domain, which would allow for the closure of the extracellular and the intracellular gates in the absence of bound substrate and ions, remain to be elucidated.

Methods

Cysteine cross-linking

Glt_{Ph}-K55C/C321A/A364C was expressed as His_8 fusion and purified as described previously[8]. Transporter samples were exchanged by size exclusion chromatography (SEC) into buffer, containing (in mM) 10 HEPES/NaOH or KOH, pH 7.4, 1 n-dodecyl-β-D-maltopyranoside and either 100 NaCl and 0.1 L-asp or 100 KCl. Cross-linking was initiated by addition of 1:2 molar ratio of Cu^{2+} and 1,10 phenantroline or $HgCl_2$. Reactions were quenched with 100 mM N-ethyl maleimide prior to SDS PAGE analysis. Crude *E. coli* membranes were isolated by centrifugation, washed either in a Na^+/L-asp-containing or free buffer and cross-linked as in detergent. Protein bands were visualized by western blotting using antibodies against histidine tag.

Crystallography

K55C/C321A/A364C mutation was introduced within a heptahistidine mutant of Glt_{Ph}, used in earlier crystallographic studies[8,9], to which we refer as “wild type” for brevity. Purified protein was cross-linked in the presence of 10 fold molar excess of $HgCl_2$, dialyzed against buffer containing 10 mM HEPES/NaOH, 7 mM n-decyl-β-D-maltopyranoside, 100 mM NaCl and 100 μM L-asp, diluted to the final concentration of 2–4 mg/ml and supplemented with 0.5 mM *E. coli* total polar lipid extract and 100 mM NaBr. Protein solution was mixed at 1:1 (v:v) ratio with the reservoir solution, containing 100 mM MES, pH 5.0, 18–20 % PEG 350 MME and 200 mM $CaCl_2$, and crystallized at 4 °C by hanging drop vapour diffusion. Crystals were cryoprotected by allowing the drop to dry until its volume was reduced by 50 %. Selenomethionine-substituted protein was expressed as described previously[8] and crystallized as above. Diffraction data were indexed, integrated and scaled using HKL-2000 package[41]. Further analyses were performed using CCP4 programs[42]. Initial phases were obtained using Phaser[43], and the protein model built manually in Coot[44] and refined using REFMAC[42] with TLS[45] and three fold NCS restrains.

Supplementary Material

Refer to Web version on PubMed Central for supplementary material.

Acknowledgments

We thank Drs. D. Patel and H. Li for the help with ITC and Dr. H. Weinstein for constructive criticism. X-ray diffraction data were measured at X25 beamline at the National Synchrotron Light Source. This work was supported by the National Institute of Health (O.B.) and by a Jane Coffin Childs Memorial Fund postdoctoral fellowship (N.R.).

REFERENCES

1. Danbolt NC. Glutamate uptake. Prog Neurobiol 2001;65:1–105. [PubMed: 11369436]
2. Saier MH Jr. Tran CV, Barabote RD. TCDB: the Transporter Classification Database for membrane transport protein analyses and information. Nucleic Acids Res 2006;34:D181–6. [PubMed: 16381841]

3. Mitchell P. A general theory of membrane transport from studies of bacteria. Nature 1957;180:134–6. [PubMed: 13451664]
4. Patlak CS. Contributions to the theory of active transport: II. The gate type non-carrier mechanism and generalizations concerning tracer flow, efficiency, and measurement of energy expenditure. Bulletin of Mathematical Biology 1957;19:209–235.
5. Jardetzky O. Simple allosteric model for membrane pumps. Nature 1966;211:969–70. [PubMed: 5968307]
6. Sobczak I, Lolkema JS. Structural and mechanistic diversity of secondary transporters. Curr Opin Microbiol 2005;8:161–7. [PubMed: 15802247]
7. Krishnamurthy H, Piscitelli CL, Gouaux E. Unlocking the molecular secrets of sodium-coupled transporters. Nature 2009;459:347–55. [PubMed: 19458710]
8. Yernool D, Boudker O, Jin Y, Gouaux E. Structure of a glutamate transporter homologue from Pyrococcus horikoshii. Nature 2004;431:811–8. [PubMed: 15483603]
9. Boudker O, Ryan RM, Yernool D, Shimamoto K, Gouaux E. Coupling substrate and ion binding to extracellular gate of a sodium-dependent aspartate transporter. Nature 2007;445:387–93. [PubMed: 17230192]
10. Yernool D, Boudker O, Folta-Stogniew E, Gouaux E. Trimeric subunit stoichiometry of the glutamate transporters from Bacillus caldotenax and Bacillus stearothermophilus. Biochemistry 2003;42:12981–8. [PubMed: 14596613]
11. Gendreau S, et al. A trimeric quaternary structure is conserved in bacterial and human glutamate transporters. J Biol Chem 2004;279:39505–12. [PubMed: 15265858]
12. Raunser S, et al. Structure and function of prokaryotic glutamate transporters from Escherichia coli and Pyrococcus horikoshii. Biochemistry 2006;45:12796–805. [PubMed: 17042498]
13. Koch HP, Larsson HP. Small-scale molecular motions accomplish glutamate uptake in human glutamate transporters. J Neurosci 2005;25:1730–6. [PubMed: 15716409]
14. Grewer C, et al. Individual subunits of the glutamate transporter EAAC1 homotrimer function independently of each other. Biochemistry 2005;44:11913–23. [PubMed: 16128593]
15. Leary GP, Stone EF, Holley DC, Kavanaugh MP. The glutamate and chloride permeation pathways are colocalized in individual neuronal glutamate transporter subunits. J Neurosci 2007;27:2938–42. [PubMed: 17360916]
16. Koch HP, Brown RL, Larsson HP. The glutamate-activated anion conductance in excitatory amino acid transporters is gated independently by the individual subunits. J Neurosci 2007;27:2943–7. [PubMed: 17360917]
17. Groeneveld M, Slotboom DJ. Rigidity of the subunit interfaces of the trimeric glutamate transporter GltT during translocation. J Mol Biol 2007;372:565–70. [PubMed: 17673229]
18. Shimamoto K, et al. DL-threo-beta-benzyloxyaspartate, a potent blocker of excitatory amino acid transporters. Mol Pharmacol 1998;53:195–201. [PubMed: 9463476]
19. Ryan RM, Mitrovic AD, Vandenberg RJ. The chloride permeation pathway of a glutamate transporter and its proximity to the glutamate translocation pathway. J Biol Chem 2004;279:20742–51. [PubMed: 14982939]
20. Manceau A, Nagy KL. Relationships between Hg(II)-S bond distance and Hg(II) coordination in thiolates. Dalton Trans 2008:1421–5. [PubMed: 18322620]
21. Dieckmann CR, et al. De Novo Design of Mercury-Binding Two- and Three-Helical Bundles. J Am Chem Soc 1997;119:6195–6196.
22. Rosenzweig AC, et al. Crystal structure of the Atx1 metallochaperone protein at 1.02 A resolution. Structure 1999;7:605–17. [PubMed: 10404590]
23. Sadeghi M, Naderi-Manesh H, Zarrabi M, Ranjbar B. Effective factors in thermostability of thermophilic proteins. Biophys Chem 2006;119:256–70. [PubMed: 16253416]
24. Grunewald M, Menaker D, Kanner BI. Cysteine-scanning mutagenesis reveals a conformationally sensitive reentrant pore-loop in the glutamate transporter GLT-1. J Biol Chem 2002;277:26074–80. [PubMed: 11994293]
25. Borre L, Kavanaugh MP, Kanner BI. Dynamic equilibrium between coupled and uncoupled modes of a neuronal glutamate transporter. J Biol Chem 2002;277:13501–7. [PubMed: 11823462]

26. Seal RP, Shigeri Y, Eliasof S, Leighton BH, Amara SG. Sulfhydryl modification of V449C in the glutamate transporter EAAT1 abolishes substrate transport but not the substrate-gated anion conductance. Proc Natl Acad Sci U S A 2001;98:15324–9. [PubMed: 11752470]
27. Ryan RM, Vandenberg RJ. Distinct conformational states mediate the transport and anion channel properties of the glutamate transporter EAAT-1. J Biol Chem 2002;277:13494–500. [PubMed: 11815608]
28. Leighton BH, Seal RP, Shimamoto K, Amara SG. A hydrophobic domain in glutamate transporters forms an extracellular helix associated with the permeation pathway for substrates. J Biol Chem 2002;277:29847–55. [PubMed: 12015317]
29. Slotboom DJ, Sobczak I, Konings WN, Lolkema JS. A conserved serine-rich stretch in the glutamate transporter family forms a substrate-sensitive reentrant loop. Proc Natl Acad Sci U S A 1999;96:14282–7. [PubMed: 10588697]
30. Grunewald M, Bendahan A, Kanner BI. Biotinylation of single cysteine mutants of the glutamate transporter GLT-1 from rat brain reveals its unusual topology. Neuron 1998;21:623–32. [PubMed: 9768848]
31. Seal RP, Leighton BH, Amara SG. Transmembrane topology mapping using biotin-containing sulfhydryl reagents. Methods Enzymol 1998;296:318–31. [PubMed: 9779458]
32. Shlaifer I, Kanner BI. Conformationally sensitive reactivity to permeant sulfhydryl reagents of cysteine residues engineered into helical hairpin 1 of the glutamate transporter GLT-1. Mol Pharmacol 2007;71:1341–8. [PubMed: 17272682]
33. Abramson J, et al. Structure and mechanism of the lactose permease of Escherichia coli. Science 2003;301:610–5. [PubMed: 12893935]
34. Yamashita A, Singh SK, Kawate T, Jin Y, Gouaux E. Crystal structure of a bacterial homologue of Na+/Cl--dependent neurotransmitter transporters. Nature 2005;437:215–23. [PubMed: 16041361]
35. Hunte C, et al. Structure of a Na+/H+ antiporter and insights into mechanism of action and regulation by pH. Nature 2005;435:1197–202. [PubMed: 15988517]
36. Shachnai L, Shimamoto K, Kanner BI. Sulfhydryl modification of cysteine mutants of a neuronal glutamate transporter reveals an inverse relationship between sodium dependent conformational changes and the glutamate-gated anion conductance. Neuropharmacology 2005;49:862–71. [PubMed: 16137722]
37. Huang Z, Tajkhorshid E. Dynamics of the Extracellular Gate and Ion-Substrate Coupling in the Glutamate Transporter. Biophys J. 2008
38. Shrivastava IH, Jiang J, Amara SG, Bahar I. Time-resolved mechanism of extracellular gate opening and substrate binding in glutamate transporter. J Biol Chem. 2008
39. Gouaux E. The molecular logic of sodium-coupled neurotransmitter transporters. Philos Trans R Soc Lond B Biol Sci 2009;364:149–54. Review. [PubMed: 18977735]
40. Ryan RM, Compton EL, Mindell JA. Functional characterization of a Na+-dependent aspartate transporter from Pyrococcus horikoshii. J Biol Chem 2009;284:17540–8. [PubMed: 19380583]
41. Otwinowski Z, Minor W. Processing of X-ray diffraction data collected in oscillation mode. Methods Enzymol 1997;276:308–326.
42. No4, C. p. The CCP4 Suite: Programs for X-ray crystallography. Acta Crystallogr. D 1994;50:760–763. [PubMed: 15299374]
43. McCoy AJ, et al. Phaser crystallographic software. J. Appl. Cryst 2007;40:658–674. [PubMed: 19461840]
44. Emsley P, Cowtan K. Coot: model-building tools for molecular graphics. Acta Crystallogr D Biol Crystallogr D 2004;60:2126–2132.
45. Winn MD, Isupov MN, Murshudov GN. Use of TLS parameters to model anisotropic displacements in macromolecular refinement. Acta Crystallogr D Biol Crystallogr 2001;57:122–33. [PubMed: 11134934]
46. DeLano, WL. The PyMOL Molecular Graphics System. DeLano Scientific LLC; Palo Alto, CA, USA: 2008.
47. Saha RP, Bahadur RP, Pal A, Mandal S, Chakrabarti P. ProFace: a server for the analysis of the physicochemical features of protein-protein interfaces. BMC Struct Biol 2006;6:11. [PubMed: 16759379]

48. Landau M, et al. ConSurf 2005: the projection of evolutionary conservation scores of residues on protein structures. Nucleic Acids Res 2005;33:W299–302. [PubMed: 15980475]

49. Finn RD, et al. The Pfam protein families database. Nucleic Acids Res 2008;36:D281–8. [PubMed: 18039703]

50. Larkin MA, et al. Clustal W and Clustal X version 2.0. Bioinformatics 2007;23:2947–8. [PubMed: 17846036]

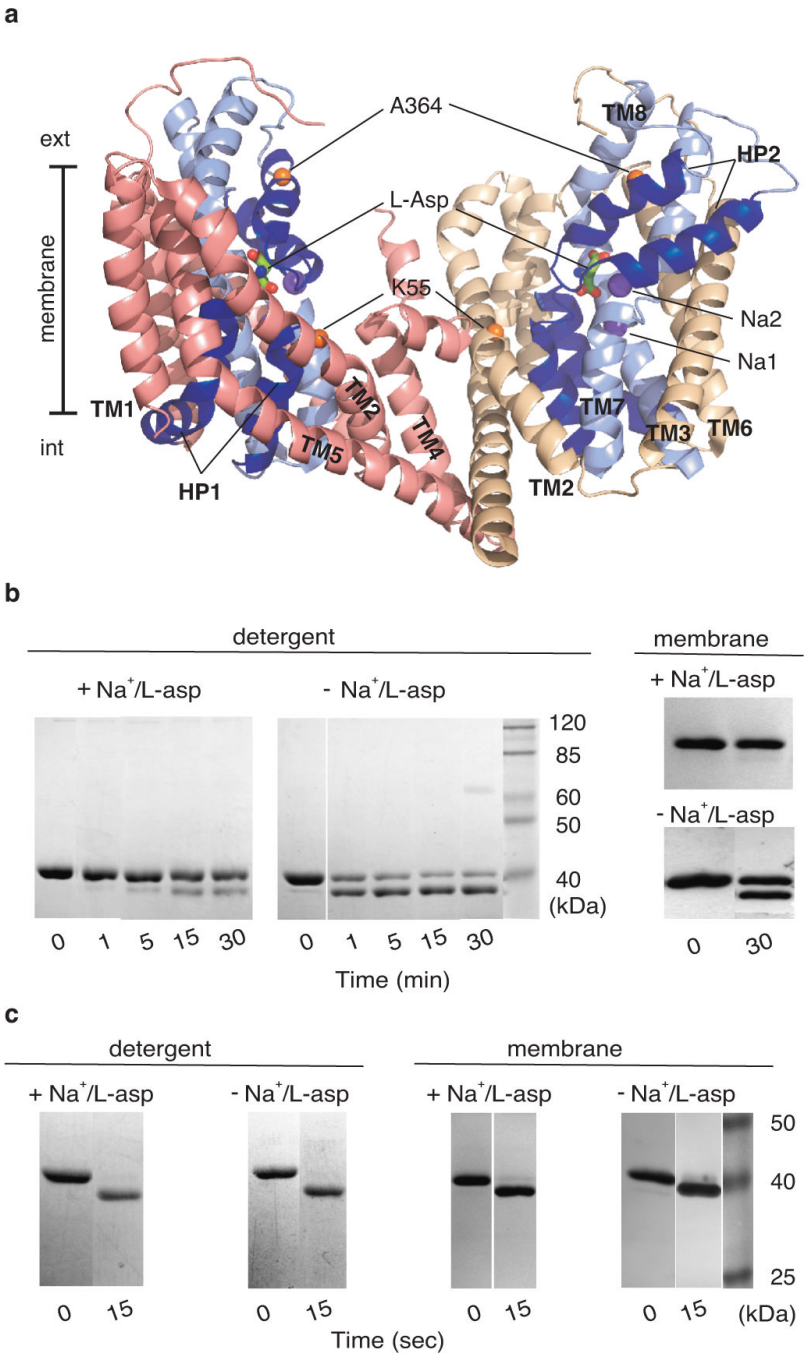

Figure 1. Cross-linking of Glt_{Ph}-K55C/A364C

a, Cartoon representation of two substrate-bound Glt_{Ph} protomers (PDB code 2NWX) viewed in the membrane plain. The third protomer and TM4 of the protomer on the right are removed for clarity. TMs 1 through 6 are coloured salmon and wheat; the carboxyl terminal cores are light blue; and the hairpins HP1 and HP2 are dark blue. Bound L-asp and Na^+ are shown as sticks and purple spheres, respectively. Orange spheres correspond to the Cα atoms of residues 55 and 364. All molecular representations have been generated using Pymol[46]. **b**, SDS PAGE analysis of Glt_{Ph}-K55C/A364C before and after incubation with 100 μM CuPhen for indicated periods of time. Detergent-solubilized purified Glt_{Ph}-K55C/A364C (left) and unpurified transporter in crude *E. coli* membranes (right) were visualized by Coomassie staining and

western blotting, respectively. **c**, Cross-linking of Glt_{Ph}-K55C/A364C in the presence of 50 μM $HgCl_2$. Samples were analyzed as in **b**.

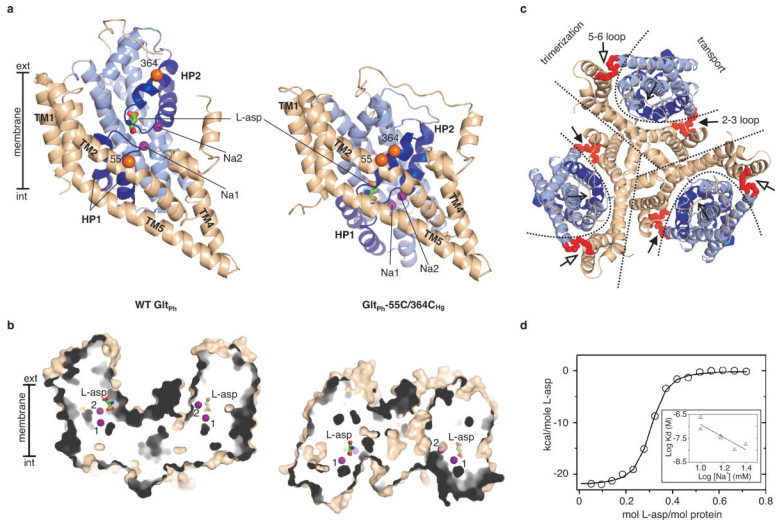

Figure 2. Glt$_{Ph}$-55C/364C$_{Hg}$ in the inward facing substrate-bound state

Cartoon representation of the single protomers (**a**) and surface representation of the trimers sliced through the binding sites (**b**). WT Glt$_{Ph}$ and Glt$_{Ph}$-55C/364C$_{Hg}$ are shown on the left and right, respectively. In (**a**), TMs 1, 2, 4 and 5 are coloured wheat with the remainder of the protomer light blue. Na^+ are shown as purple spheres. **c,** Extracellular view of Glt$_{Ph}$-55C/364C$_{Hg}$ with straight and curved lines delineating individual protomers and transport domains, respectively. The trimerization domains (wheat) and transport domains (blue) are connected by short cytoplasmic (solid arrows) and extracellular (open arrows) loops, highlighted in red. The long TM3–4 loops (simple arrows) cross over the transport domains. **d**, Isothermal titration calorimetry analysis of L-asp binding to Glt$_{Ph}$-55C/364C$_{Hg}$. Shown are the binding heats in 10 mM NaCl. The linear dependence (slope = −2.6 ± 0.7) of the *log* of the apparent dissociation constant, K_d, on the *log* of Na^+ concentration is shown in the inset. Glt$_{Ph}$-55C/364C$_{Hg}$ was exchanged into Na^+/L-asp-free buffer, diluted to 15–20 μM in the reaction cell of the Microcal ITC200, supplemented with indicated concentrations of Na^+, and titrated with L-asp at 25 °C. The binding enthalpy and the apparent number of binding sites were 23.6 ± 0.8 kcal/mol and 0.4 ± 0.03 (n=6), respectively.

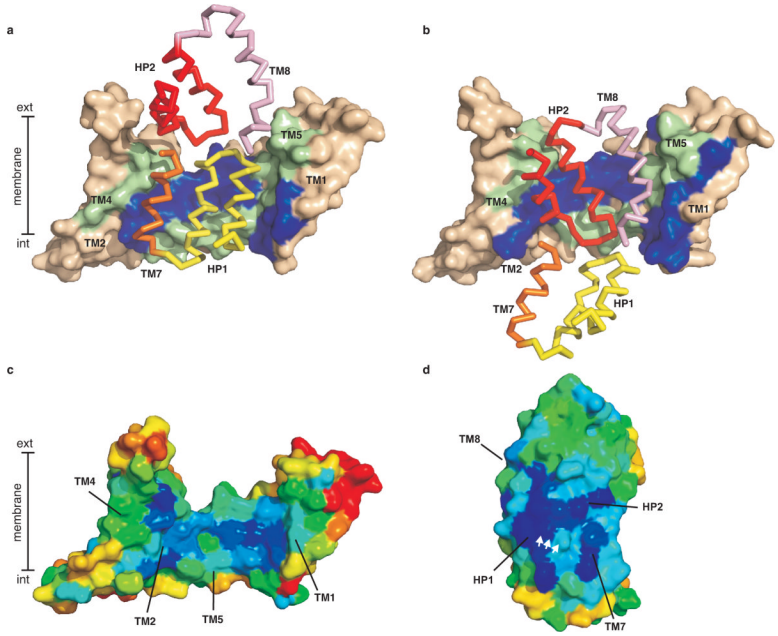

Figure 3. Domain interaction surfaces

Trimerization domains of WT Glt_{Ph} (**a**) and Glt_{Ph}-55C/364C_{Hg} (**b**) are shown in surface representation and coloured wheat. Residues involved in domain contacts, identified by ProFace server[47], are coloured blue (TM1 and 2) and green (TM4 and 5). Interacting structural elements of the transport domain are shown in ribbon representation: HP1 (yellow) and TM7 (orange) in WT Glt_{Ph}, and HP2 (red) and TM8 (pink) in Glt_{Ph}-55C/364C_{Hg}. Surface representation of the trimerization (**c**) and transport (**d**) domains coloured according to evolutionary conservation. Dark blue and red correspond to the highly conserved and variable residues, respectively. The interacting surfaces are facing the viewer and the white arrows mark the highly conserved serine-rich signature motif in HP1. Conservation scores were calculated using Consurf server[48] and 212 SLC1 sequences with less than 60 % identity harvested from Pfam database[49] and aligned in ClustalW2[50].

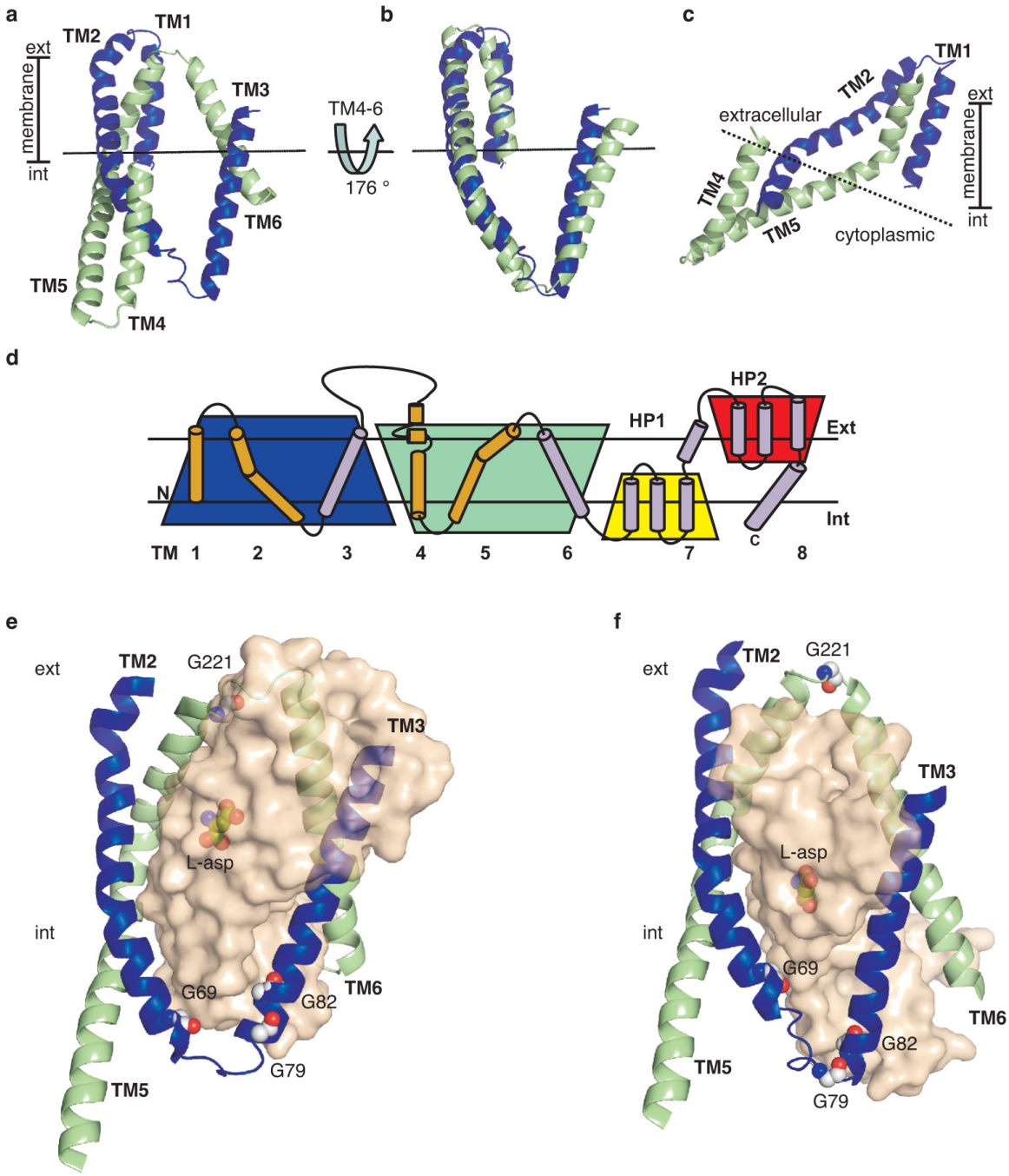

Figure 4. Amino-terminal inverted structural repeat

Cartoon representation of TMs 1–3 (blue) and TMs 4–6 (green) in the Glt_{Ph}-55C/364C_{Hg} viewed in the membrane plain (**a**), and their structural superposition (**b**). **c**, Symmetrical helices, TMs 1–2 and TMs 4–5, form the interaction surface within the transport domain, which is partitioned into intracellular and extracellular halves delineated by the dotted line. (**d**) Schematic representation of Glt_{Ph} trimerization (orange) and the transport (light blue) domains. Two inverted structural repeats are emphasized by blue and green, and yellow and red trapezoids. Structure of TM2–3 and TM5–6 loops in WT Glt_{Ph} (**e**) and Glt_{Ph}-55C/364C_{Hg} (**f**). TMs 2 through 6 are shown in cartoon representation with 4 omitted for clarity. The

transporter core is shown in transparent surface representation. Bound L-asp and the highly conserved glycines are shown as spheres.

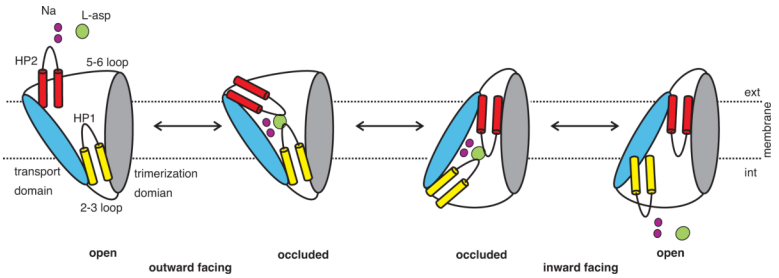

Figure 5. Schematic transport mechanism

Shown is a single transporter protomer. Substrate and sodium binding to the outward and inward facing states is coupled to the closure of the extracellular and intracellular gates, HP2 (red) and HP1 (yellow), respectively. Isomerization between the outward and inward facing occluded states occurs upon movement of the transport domain (blue), relative to the trimerization domain (grey). The inward facing open state has not been structurally characterized and is hypothetical.